



The mechanisms of controlling FCT life and failure mode of Ni-based EBPVD YSZ thermal barrier coatings via the effects of both substrate elements and reactive element doping

Klaus Fritscher¹

Received: 1 September 2020 / Accepted: 18 November 2020

© The Author(s) 2020

Abstract

Electron-beam physical vapor deposition (EBPVD) of NiCoCrAlY- and Hf-modified bond coats on (1) selected polycrystalline, directionally solidified, (2) single crystalline substrate alloys and (3) an uncoated NiCrAl bond-coat surrogate substrate, all of them covered with standard EBPVD YSZ topcoats were subjected to cyclic furnace testing (FCT) at 1100 °C. The lifetime and spallation failure upon FCT were evaluated. A typical mixed layer zone (MZ) of alumina and zirconia has formed during topcoat processing above the thermally growing oxide layer. The MZ was investigated by energy-dispersive X-ray spectroscopy after intermediate lifetimes and at the end of life. Chemical composition of the MZ and lifespan data were related to each other thus accounting for rate-determining reactions which could be assigned to either cation- or anion-controlled transport mechanisms. These provide a new approach to address FCT life and failure mode of even complex TBC systems containing reactive elements (e.g. Y and Hf). The cation-controlled processes are accelerated according to their concentration by tetravalent elements of the substrates, while the anion-controlled processes are unaffected by this and only adopt a cation-dominated mode when alloying elements of a low valence (e.g. Ti⁺) reach a supercritical concentration.

Keywords Thermal barrier coating · Thermally grown oxide · Electron-beam physical vapor deposition (EBPVD) · Reactive element effect · Substrate effect

1 Introduction

Thermal barrier coating systems (TBCs) are applied on the superalloy components in the hot sections of gas turbines used in aviation, maritime mass transport and electrical power generation. Thanks to the effect of the thermal protection system, higher service temperatures are reached during combustion thus enabling extremely high levels of efficiency.

From the 1950s, the industrial process of precision investment casting of alloys under vacuum unleashed the development of superalloys. Targeted development of high-temperature alloys, preferably Ni-based, both alloyed

with γ' precipitation-hardening and/or refractory element solution-hardening alloy additions, gave them the opportunity to operate at a high fraction of their melting points in the engine. The processing of monocrystalline or directionally solidified blades and vanes resulted in more high-temperature creep resistant components. Internally cooled turbine blades that allowed higher operating temperatures have been made possible by advanced machining techniques. The high operating temperatures of the components and their unsatisfactory oxidation resistance, however, especially during the cyclical use of aircraft turbines, initiated the development and application of oxidation resistant coatings in the 1960s. The so-called “reactive

✉ Klaus Fritscher, klaus.fritscher@goetttersiedlung.de | ¹DLR German Aerospace Center, Institute of Materials Research, 51170 Cologne, Germany.



element effect" (REE) proved helpful in achieving this goal. The effect was discovered more than 80 years ago in 1937 [1] probably as a result of a casting process projected for the manufacture of heating elements as the melt has been deoxidized and desulfurized by adding rare-earth elements [2]. The alloying with these elements improve the oxide adhesion of alumina/chromia forming alloys and extend their service life. Remarkably, in the period from 1939 onwards, the development of aircraft jet engines by the pioneers H.J. Pabst von Ohain and Frank Whittle (first flight of a He 178) paved the way to success. Typical oxidation protective coatings include MeCrAlY, Me = Ni and/or Co.

Ceramic protective layers are essential in order to protect the underlying metal structures from the intense heat of combusted jet fuel. The search led to the discovery of 6–8 wt% Y_2O_3 in ZrO_2 (YSZ) in 1978 [3]. The new YSZ ceramic coatings required suitable adhesive coatings on the metal base. This function could be fulfilled by the conventional oxidation resistant coatings, apart from minor processing modifications. Their name has only been changed to bond coats. When exposed to high temperatures, a protective oxide layer grows as an intermediate layer between the bond coat and the YSZ thermal barrier coating. The thermal barrier coating system thus includes all areas between the superalloy matrix and the YSZ topcoat.

Whereas the mechanism of the oxidation of alloys at elevated temperatures could already be modeled during the early 1930s by disorder reactions in the lattice of semi-conducting oxides [4], the mechanism effective during REE doping is still under investigation. This is basically due to the complexity of the reactive element effect. The list of its beneficial effects includes

1. Promoting the selective oxidation of Al.
2. Reducing the scale growth rate.
3. Improving the scale adhesion.
4. Changing the scale growth mechanism from predominantly outward to oxygen inward transport.

While different processing methods for the large-scale coating of superalloy components with bond coats and YSZ topcoats exist, this study only focuses on the application of overlay coatings in order to limit the amount of processing parameters.

Bond coat overlay coatings basically consist of the chemical elements MCrAlRE, M = Ni and/or Co, RE = reactive elements e.g. Y and/or Hf. They are mainly plasma spray deposited (PS) in a low-pressure atmosphere or otherwise applied via electron-beam physical vapor deposition (EBPVD) in vacuum. Generic research on protective oxide adherence and manufacturing processes of contemporary

types of protective coating systems are addressed by Goward [5].

The two types of overlay bond-coat layers differ basically because of their different genesis: Plasma spray (PS) layers grow by impacting liquid and/or semi-liquid spray powder particles on the component. Liquid phase segregation and transition phase effects due to rapid quenching are likely. In contrast, EBPVD layers form by solid-state deposition from the gas phase: they grow steadily in thermodynamic equilibrium via sublimation/nucleation steps. The deposition of the metallic layers from the vapor phase is due to nucleation, which results in directional columnar structures during growth. These need to be compacted, e.g. via zircon ball peening, in order to minimize the surface area of the bond coat. Subsequent vacuum annealing reintroduces the original flat surface of the substrate.

YSZ ceramic topcoats are deposited on the pre-prepared bond coats using a slightly modified EBPVD process. The YSZ deposition occurs in a controlled atmosphere of oxygen bled into the deposition chamber. The gaseous zirconia molecules condense and grow at about 1000 °C to columnar feather-like zirconia structures on the bond-coated substrates. The concurrent oxidation reaction of the bond coat of outward-growing transient alumina is interacting with the impinging zirconia/yttria vapor molecules and initiates partial dissolution of the YSZ in the outer layer of the transient oxide phase. This so-called "mixed zone" (MZ) forms during a transition period where outward growing transient γ or θ or spinel phases and condensing YSZ vapor meet. They stop growing when they transform into stable inward-growing α -alumina matrix together with the imbedded YSZ precipitates. This phase transformation is complete at the end of the coating process, thereby achieving a constant layer thickness [6, 7]. The nanometer-sized MZ ensures a thermodynamically and mechanically stable bond to both the stable α -alumina-based TGO below and to the YSZ topcoat above. In addition, the MZ is in equilibrium with the atmosphere above and provides the unimpeded supply of oxygen (Fig. 1).

The *lifetime and failure* of TBCs in the FCT (cyclic furnace test) relate to multiple failure modes and mechanisms which have to be solved individually. As a widespread cause of failure of thermally grown oxide layers by chipping, the effects of compressive stresses in the TGO have been addressed [9]. The mechanisms of separation failure are attributed to non-planarity of the Me/TGO interfaces, which generate (mechanical) fatigue cracks under cyclic loading in the boundary region. These grow in a wedge-shaped mode along the TGO/Me interface under the influence of thermal cycling [10]. The origin of the separations is not completely understood. Stress and strain assessments within layer systems have stimulated a fracture

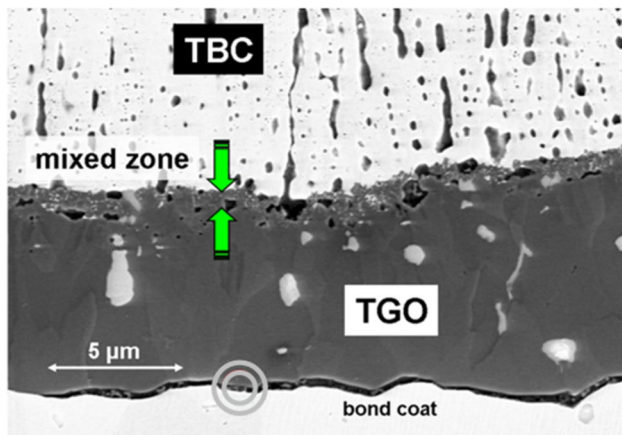


Fig. 1 Typical mixed zone (MZ) presented in a standard EBPVD NiCoCrAlY bond-coated IN100 TBC system after FCT separation failure at the Me/TGO interface at end of life after 1250 cycles alias 1042 hot hours at 1100 °C (SEM micrograph, courtesy W. Braue) [8]. The 1.5 μm thick MZ between YSZ TBC topcoat (above) and columnar alumina zone (CAZ) of the TGO (below) is indicated by arrows. YAG precipitates (light grey) are imbedded in the TGO. Spinel phase located within the separation crack is marked by circles

mechanistic view of failure processes. From this predictive lifetime estimates have been derived which are likely to apply to the vast majority of PS bond-coated TBC systems.

The mechanistic failure approach [11, 12] has also been tentatively transferred to EBPVD NiCoCrAlY bond-coated TBC systems [13]. The failure of TBC systems, whose YSZ topcoat was alternatively manufactured using PS and EBPVD processes on PS-generated bond coats, were discussed in a comparative manner. Their lifetime and respective failure modes depend on several parameters e.g. structure of the bond coat and FCT frequency [14].

In contrast to the mechanistic perspective to life prediction of PS bond-coated TBC systems, the chemical composition of the MZ of EBPVD bond-coated TBC systems

has recently been proven as a significant indicator of the service life [15]. This approach can also be applied to no-bond-coat TBC systems [16].

Essential differences in processing and process-related influencing between PS- and EBPVD-made bond coats in TBC systems are listed in Table 1.

By comparing the well-documented damage behavior and the lifespan of PS- and EBPVD-based TBC systems, initial conceptions can be drawn about the mechanisms of nucleation and adhesion (Table 2).

For this study the following six TBC systems were employed as bond-coated substrates or as bond coat surrogates, each top-coated with a standard EBPVD YSZ layer for FCT experiments. Standard NiCoCrAlY bond coats and Hf-modified NiCoCrAlY coatings were used as bond coats.

- DS eutectic NiCrAl → bond coat surrogate alloy.
- EB remolten NiCoCrAl + Y → MCrAlY.
- SX solid-solution-strengthened superalloy → CMSX-4.
- DS precipitation-hardening superalloy → IN100.
- DS superalloy + Hf → MarM002.
- DS solid-solution-strengthened superalloy + Hf → René 142.

The study is addressing the mechanisms imposed by the effects of both (1) the substrate alloy compositions and (2) reactive element doping involvement on cyclic life and failure mode for YSZ top-coated no-bond-coated, NiCoCrAlY-bond-coated and NiCoCrAlYHf-bond-coated substrates. It is an extension of previous work at DLR [15] to a now larger variety of different TBC systems emphasizing again the chemical composition of the MZ as a sensitive indicator of service life.

Lifetimes at temperature and adhesion performance are correlated with corresponding chemical data of the MZ in order to derive transport relationships. They will be

Table 1 Coating process related differences between PS- and EBPVD-made bond coats

Category	PS	EBPVD
Substrate surface pretreatment prior to bond coat processing	Grit blasting	Smoothing
Oxygen content in as-coated bond coat	~ 1000 ppm	~ 10 ppm
Structure of TGO layer near the BC/TGO interface	Undulated	Flat
Formation of a uniform mixed zone interlayer	No	Yes

Table 2 Key issues for PS- and EBPVD-made TBC systems related to the adhesion of coatings

Special features	PS TBCs	EBPVD TBCs
1. Influence of substrate surface roughness on life	Unspecific	Decisive
2. CTE mismatch between substrate and TGO	Yes	No effect
3. Dependency of FCT frequency on lifetime	Yes	No effect
4. Site of failure at end of life	Unspecific	At Me/TGO interface
5. Lifetime predictions refer to	Mechanics	Chemistry

assigned by means of point defect thermodynamics to life-determining transport processes in the TGO. The focus is on the extent to which the thermodynamics of the transport processes in the α -alumina crystal lattice describe the various effects of the reactive elements on EBPVD TBC systems in order to shed light on the very mechanisms being effective.

2 Experimental procedures

2.1 Substrate materials as a base for TBC systems

The composition of the substrate alloys of this study are given in wt% in Table 3.

The DS NiCrAl material of ternary eutectic composition is acting as a bond coat surrogate. The DS NiCrAl bars have been manufactured by a Bridgman crystal growth process. This procedure resulted in a lamellar unidirectional arrangement of 68 vol% γ -Ni phase and 32 vol% of interconnected β -NiAl- and α -Cr-phase. The center distance between the γ -Ni lamellae is 12 μm [17]. Disc-shaped coupons were spark-erosion cut from the bars parallel and transverse to the alignment of the phases.

2.2 Bond coating manufacture

The Ni-base IN100, CMSX-4 and MCrAlY substrates employed for TBC deposition are made via machining of precursor materials to cylindrical samples exhibiting a R_a 0.15 surface finish. They received standard 100 μm thick EBPVD bond coats (nominal composition in wt%: Ni–21Co–19Cr–12.5Al–0.15Y) in a 60 kW coater (Leybold). Two corresponding individual samples René 142 and MarM 002 with same bond coat composition are assigned to these batches. They belonged to separate examinations within FCT campaigns that were only temporarily available for EDS examinations.

A test series of IN100 and CMSX-4 samples was provided for applying Hf-modified NiCoCrAl-base bond coats using a method of jumping-beam evaporation from a dual source in a 150 kW coater (von Ardenne) [16]. For this purpose, extra-long “duplicate samples” have to be provided.

So an alternative production step of round machining of the samples by centerless grinding was required due to their excessive diameter to length ratio of 1:20 leading to a super-finish of R_a 0.006 over the whole length. These sample substrates got a modified bond coat composition of the reactive elements Y + Hf of (a) 0.11 wt% Y (0.07 at% Y) + 1.2 wt% Hf (0.35 at% Hf) and of (b) 0.11 wt% Y (0.07 at% Y) + 0.6 wt% Hf (0.18 at% Hf).

An IN100 sample with an atypical super-finish of R_a 0.006 was supplied and bond-coated with an unusual Cr-rich NiCoCrAlY composition of 30 wt%. This individual sample resulted from a preliminary test run to set up the optimal local positioning of samples within the coating chamber above the quinary NiCoCrAlY evaporation pool in order to be able to produce standard bond coat compositions.

The initial sparse structures of the bond coats in the as-coated state generally need a physical and thermal post-treatment for densification which is routinely done via shot peening with suitable materials e.g. zircon balls followed by a vacuum anneal for 4 h at 1080 °C. The DS NiCrAl coupons acting as BC surrogates were un-peened in order to preserve their special eutectic structure.

2.3 YSZ thermal barrier topcoat manufacture

The uncoated, NiCoCrAlY-coated and Hf-modified NiCoCrAl-base bond coats were top-coated with standard YSZ. They were deposited by standard “reactive” EBPVD processing in a 150 kW coater (von Ardenne) at 1000 °C.

2.4 Isothermal oxidation testing of DS NiCrAl bond coat surrogate

Isothermal oxidation kinetics of the DS NiCrAl bond coat surrogate in the uncoated state at 1100 °C parallel and transverse to the fiber orientation were conducted to investigate the individual oxidation behavior of the surfaces experimentally in 100 h tests aimed at their suitability as a TBC substrate [18].

Table 3 Substrate alloys of the TBC systems of this study. Composition in wt%, nickel is balance

Alloy	Fabrication	Co	Cr	Al	Mo	W	Ta	Ti	Hf	Re	C	B	Others
Ni–Cr–Al	DS via Bridgman		37.5	7									
IN 100	DS	14	9	5	2.3			5			0.18	0.015	0.05 Zr, 1 V
CMSX-4	SX'tal	9	6.5	5.6	0.6	6	6.5	1	0.1	3			
MCrAlY	VIM + EBR	22.2	19.8	12.2									0.35 Y
René 142	DS	12	6.8	6.1	1.5	4.9	6.3		1.2	2.8	0.12		≤0.02 Zr
MarM 002	DS	10.1	8.9	5.8	0.1		2.5	1.5	1.5		0.13		0.03 Zr

2.5 FCT (Cyclic furnace testing)

In real cases, turbine components are subject to exposure to the oxidative hot gas jet at up to 30 atm pressure. These conditions are simulated in cyclic burner rig tests. In addition, the cyclic furnace tests (FCT) have become popular under laboratory conditions in ambient laboratory air. They largely meet the decisive requirements for metallic components in a gas turbine, namely thermal fatigue which is the primarily life-determining failure mechanism.

Standard FCT intervals are 50 min at temperature (typically 1100 °C) and 10 min cool down to RT in agitated air. The tests were usually conducted on 6 mm diameter cylindrical samples showing a diameter to length ratio of 1:10. The lifetimes *alias* hot hours of the TBC systems are investigated in previous work [15, 16] and in this study.

3 Results

3.1 FCT lifetime and MZ content of DS NiCrAl bond coat surrogate TBC system

The substrate is a directionally solidified ternary Ni–Cr–Al eutectic showing a strongly anisotropic structure of α -Cr, β -NiAl and γ -Ni phase. A few samples of transverse orientation to the longitudinal DS structure have received a YSZ topcoat. They represent a no-bond-coat TBC system. They were untypically tested to FCT at 1100 °C in cycles of 30 min holding period. A service life of one cycle *alias* ½ h was determined [16]. The MZ after two ½ h cycles *alias* 1 hot hour at 1100 °C was investigated. It revealed a relatively high Cr content of 20.59 at%. The MZ content is given in Table 4. The MZ thickness on the DS NiCrAl

sample after FCT subjected for one hour at 1100 °C was about 0.25 μm .

3.2 Isothermal oxidation of DS NiCrAl bond coat surrogate

The isothermal oxidation kinetics of the uncoated material have been recorded for 100 h at 1100 °C parallel and transverse to the alignment of the DS structural orientation. The parallel oriented material displayed early spallation of the scale whereas the sample showing transverse orientation displayed superior parabolic oxidation behavior and a persistent protective scale formation according $k_p \sim 1.174 \cdot 10^{-12} \text{ g}^2 \text{ cm}^{-4} \text{ s}^{-1}$ [18]. Oxidation kinetics transverse to the DS structural orientation is approximated by $\Delta m = m_0 + \sqrt{k_p} \cdot \sqrt{t}$.

$$m_0 = 6.87 \times 10^{-6} \text{ g cm}^2,$$

$$k_p = 1.174 \times 10^{-12} \text{ g}^2 \text{ cm}^{-4} \text{ s}^{-1}.$$

3.3 FCT lifetime and MZ content of

- of DS NiCrAl surrogate TBC system after 1 h and
- of NiCoCrAlY bond-coated TBC systems after 417 h.

The MZ of TBC samples being FCT subjected for 417 h (500 cycles) at 1100 °C has been analyzed by SEM/EDS. Instead of analyzing phases, the composition of the surface area was carried out in the middle of the MZ in order to obtain an average value for the MZ. A high level of accuracy, even for small contents, was aimed for by means of long EDS measuring times. The samples formed a TGO by FCT; the NiCoCrAlY bond-coated samples showed a MZ of up to about 1.5 μm thickness on the upper periphery of the TGO. The MZ thickness of the no-bond-coated DS NiCrAl

Table 4 FCT times at temperature (hot hours at 1100 °C), related relative lifetimes of the analyzed samples (bold numbers) and EDS data of the MZ (at%, balance is Al and O)

TBC system	Hot hours/relative lifetime	Cr	Y	Zr	Other elements	References
<i>Without bond coat</i>						
Ni–Cr–Al/YSZ	1 2	20.0	0.78	4.32	0.7 Ni	[16]
<i>Bond-coated</i>						
IN100/NiCoCrAlY/YSZ	417 0.758	0.45 ± 0.04	1.58 ± 0.47	1.49 ± 0.61	≤ 0.2 Co ≤ 0.15 V	[15]
CMSX-4/NiCoCrAlY/YSZ	417 1.33	0.22 ± 0.09	1.64 ± 0.45	2.58 ± 0.42		[15]
MCrAlY/NiCoCrAlY/YSZ	417 0.235	0.21 ± 0.10	0.96 ± 0.38	0.84 ± 0.33		[15]

FCT failure of a non-standard IN100 substrate TBC system with an atypical super-finish of R_a 0.006 containing 30 wt% Cr instead of 19 wt% Cr in the bond coat occurred after 363 cycles *alias* 280 hot hours at 1100 °C

TBC sample, which has been FCT subjected for one hour at 1100 °C, was about 0.25 μm. The EDS data of the MZ are compiled in Table 4 as a function of the time at temperature as well as the “relative lifetime” given in bold numbers.

3.4 Time at 1100 °C (hot hours) and MZ content of

- (a) standard NiCoCrAlY bond-coated Hf-alloyed substrate TBC systems and
- (b) modified NiCoCrAlYHf bond-coated TBC systems (Table 5)

3.5 FCT lifetime of TBC systems with Hf-modified NiCoCrAlY bond coats

The lifetimes refer to the effect of substrates of solid-state solution strengthened CMSX-4 and precipitation-hardening IN100 superalloys (Table 6).

4 Discussion

Thorough discussion of the effects of substrate elements versus reactive element doping on FCT life and failure mode from the six Ni-based EBPVD-TBCs as investigated in this study is organized as follows:

The effects of substrate elements (Ni, Cr, Al) are addressed the Sects. 4.1 (oxide formation at the Me/TGO interface related to surface morphology), 4.2 (adhesion issues) and 4.3 (Cr effects in the bond coat and the TGO) respectively.

Along with several subsections the effects of reactive element doping are discussed in Sects. 4.4 (Y-doping) and 4.5 (Hf-doping) respectively.

4.1 Surface morphology favoring nucleation of oxides at the Me/TGO interface detrimental to adhesion

The production of EBPVD systems is based on the following process steps (1) provision of components made of high-temperature superalloys, (2) EBPVD bond coat deposition, and (3) EBPVD YSZ topcoat deposition. Significant intermediate steps are often not mentioned. A particular step between positions (1) and (2) should be emphasized, which is already addressed in Table 1: the “smoothing” substrate surface pretreatment prior to bond coat processing. The FCT lifetime (hot hours at 1100 °C) of standard finish pretreated IN100 TBC systems of 550 h was extended according to reporting to 1185 h as soon as the same samples were given a 4000 grit super finish [19]. Comparable studies with

Table 5 FCT times at temperature (hot hours at 1100 °C), number of cycles (in bold letters), and related EDS data of the MZ (at%, balance is Al and O)

TBC system	Hot hours/number of cycles	Cr	Y	Zr	Other elements	References
<i>(a) Hf alloyed DS superalloys with standard NiCoCrAlY bond coat</i>						
René142/NiCoCrAlY/YSZ	1695/ 2034	0.89±0.66	0.82±0.54	3.12±0.35	0.09 Hf±0.06	Study
MarM 002/NiCoCrAlY/YSZ	935/ 1122	0.5±0.14	1.24±0.24	4.58±0.88	0.05 Hf±0.04	From parallel study
<i>(b) Superalloys with Hf-modified NiCoCrAlY bond coat</i>						
CMSX-4/NiCoCrAlYHf/YSZ	2587/ 3105	0.67±0.22	0.08±0.08	1.67±0.31	0.16 Hf±0.09	This study

Table 6 FCT cycles to failure for the NiCoCrAlYHf bond-coated TBC system on CMSX-4 and IN100 substrates at 1100 °C, and on CMSX-4 at 1150 °C, and calculated activation energy of lifetime (given at the right)

Thermal barrier coating system			Cycles to failure Hot hours	Cycles to failure Specified	Activation energy of lifetime (kJ mol ⁻¹)	References
Substrate	EBPVD bond coat	EBPVD top coat				
CMSX-4	NiCoCrAlYHf	YSZ	1100 °C: 5460 (± 19.5%) 4550	4426 (0.35 at% Hf); 5406 (0.18 at% Hf); 6549 (0.18 at% Hf)	474	This study
			1150 °C: 1273 (± 19.6%) 1061			
IN100	NiCoCrAlYHf	YSZ	1100 °C: 912 760	912 (0.18 at% Hf)		This study

IN100 substrates that had gotten a super finish through centerless grinding showed roughly the same improvement with a doubling of service life [20].

The preceding mechanical surface treatment of the substrates represents an integral process step which is intended to eliminate tips and ridges as potential nucleation sites for the formation of undesirable artifacts. The high energy and surface diffusion of atoms at ridges or tips or spherical powder particles is the driving force for sintering processes in the manufacture of components from powdered starting materials e.g. detailed in [21]. The excessive energy term per atom at a ridge or tip depends on the inverse of the radius of this site. The effects of atoms at the spherical site leads to an energy increase that is effectively the same as a stress or pressure working against the growth of the volume. These general statements made about the increased action of atoms in the sphere-shaped surfaces of solid material lead to specific statements e.g. in the case of an oxidizing bond coat surface: the unspecified atoms in the sphere-shaped surfaces are most likely atoms or anions of oxygen. Their amount is to be assigned to a corresponding gas pressure p_{O_2} . So a rough spike at the interface displaying a minute radius r at the tip is inversely related to the oxygen pressure at this site according to

$$\Delta p_{O_2} \sim 1/r. \quad (1)$$

Thus the increasing pressure Δp_{O_2} at a Me/TGO interface is postulated as a failure-relevant issue in YSZ TBC systems. The relevance of p_{O_2} is confirmed by experimental evidence of spinel oxides in the interior of associated pores [22].

Due to its impact on

- the concentration of alloying elements in the substrates,
- the concentration of reactive elements in the bond coats or in the substrate alloys, and
- the type of rate-determining transport mechanisms via cation or anion vacancies,

the oxygen partial pressure in TBC systems is rightly considered a crucial parameter with respect to adhesive strength and service life.

4.2 Adhesion strength between DS NiCrAl bond coat surrogate and TGO

The structure of a directionally solidified (DS) NiCrAl eutectic alloy as part of a model YSZ TBC system allows to obtain individual information on the adhesion of

interfaces both of β -phase/TGO and γ -phase/TGO [17]. The characteristics of this material are:

- The alloy is devoid of the influence of reactive elements. No foreign elements can interfere at the metal phases/TGO interfaces.
- The dominating phases for TGO formation are β -NiAl and γ -Ni. Both phases are alumina formers.
- Microstructurally both phases occur next to one another representing a heterogeneous thermodynamic system in contact with the growing TGO.

With respect to a thermodynamic perspective, the chemical potentials μ of different solid phases in a heterogeneous system are equal across phase boundaries. This topic is addressed in the Gibbs–Duhem equation according

$$n_1 d\mu_1 + n_2 d\mu_2 = 0. \quad (2)$$

The equation states that the chemical potentials μ and plausibly also the oxygen potentials p_{O_2} of β -NiAl and γ -Ni₃Al at the Me/TGO interface are different. The p_{O_2} at the Me/TGO interface is lower for β -NiAl than for γ -Ni phase.

During the YSZ coating procedure via reactive EB-PVD, a continuous TGO creating a MZ of about 0.25 μm thickness has been formed. The individual bond strengths were assessed in final FCT routes and showed a superior adhesion of the β /TGO interface compared to that of γ /TGO. The FCT induced separation progress at the Me/TGO interface documented the superior adhesion of the β -NiAl/TGO interface while the adjoining γ -Ni/TGO interface had detached. In this respect, a longer service life of a TBC system (= corresponding to better adhesion) correlates with a lower p_{O_2} at the Me/TGO interface. The lower p_{O_2} of β -NiAl exerts a stabilizing effect on the constant growth of stable α -alumina and counteracts the formation of “weak” spinel phases at the β /TGO interface.

4.3 The Cr content in DS NiCrAl bond coat surrogate and TGO

4.3.1 Effect of Cr on isothermal and cyclic oxidation performance

According to literature data of the parabolic oxidation rate constants for Ni₃Al and NiAl are raised in proportion to their Cr contents [23, 24]. The isothermal oxidation rates of the DS NiCrAl ternary eutectic Ni_{49.2}Cr_{37.5}Al_{13.3} alloy transverse to the alignment of the phases [18] are raised likewise by a factor of three compared to the

binary Ni_3Al alloys. (This increment will subsequently be indicated in a diagram comparing reference values of oxidation rate constants k_p of Ni–Al based alloys in Fig. 2.).

The higher oxidation rates of Cr alloyed NiAl alloys are not caused by a higher concentration of cation vacancies but by the cation self-diffusion in $\alpha\text{-Al}_2\text{O}_3$ where Cr^{3+} ions on the Al^{3+} ions site are active. Their diffusion characteristics, however, differ. A high dynamic participation of Cr cation transport is suggested by the lower activation energy for Cr^{3+} tracer diffusion in α -alumina of 265 kJ mol^{-1} [24] compared to a higher value for Al^{3+} self-diffusion of 382 kJ mol^{-1} [25]. Thus the different cation mobility of Al^{3+} and Cr^{3+} in $\alpha\text{-Al}_2\text{O}_3$ accounts for both the faster TGO growth rates and shorter lifetimes.

In the absence of reactive elements, the oxidation is characterized by mixed mode growth of anion and cation vacancies. The Cr content in the MZ of ~ 20 at% accumulated after 1 h of FCT submission (2 cycles of 30 min each) to 1100°C is up to two orders of magnitude higher than in all comparative samples presented in the following.

In summary, the MZ from the DS NiCrAl bond coat surrogate comprises the following characteristic features:

1. The width of this MZ (about $0.25 \mu\text{m}$) is about five times thinner than in all different remaining TBC samples (about $1.5 \mu\text{m}$).

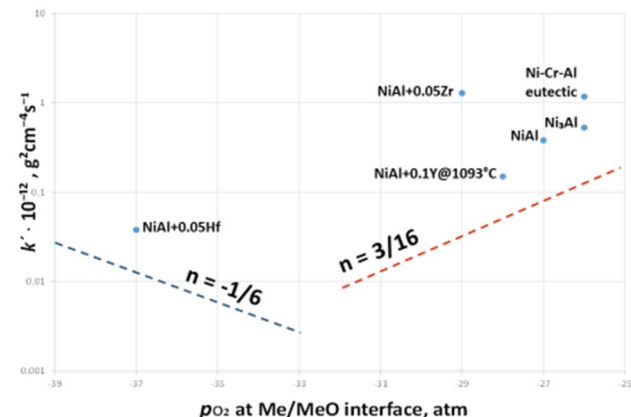


Fig. 2 Chart of the oxygen pressures at the growth front of alumina forming “binary” NiAl alloys at 1100°C versus the respective experimental parabolic oxidation-rate constants of these alloys. The dotted lines indicate the oxygen pressure dependency versus the parabolic oxidation rate constants according to Eqs. (4) and (5). Rate constants are given for Ni_3Al [23], NiAl [25], NiAl+0.1 at% Y at 1093°C [39], which each refer to a p_{O_2} according to [28, 38], NiAl+0.05 at% Zr [41] and NiAl+0.05 at% Hf [40] cataloged at 10^{-37} atm [37]. Due to its low Al content, the ternary NiCrAl eutectic $\text{Ni}_{49}\text{Cr}_{37.5}\text{Al}_{13.5}$ has been approximated to the p_{O_2} of Ni_3Al [18]

2. The Cr content of ~ 20 at% in the MZ at end of life is about two orders of magnitude higher than that in the MZ of all TBC samples having standard bond coats.
3. The FCT lifetime of 0.5 h is extremely short [16]. The cyclic lifetime is limited by separation failure at the Me/TGO interface. On the other hand, the life of a duplicate sample (without a zirconia topcoat) has not failed on isothermal heating at 1100°C in air for 100 h: it suggested good adhesion between $\alpha\text{-(Al,Cr)}_2\text{O}_3$ and $\beta\text{-NiAl}$ phase under isothermal conditions. The lifetime in isothermal oxidation mode is at least 100 times longer than in FCT mode [18].

Obviously MZ thickness, MZ composition and TBC lifetime respectively are interrelated thus calling for a broader in-depth discussion of nucleation, growth kinetics and phase reactions.

Referring to the low MZ thickness as compared to the $1.5 \mu\text{m}$ typically revealed for other systems (Fig. 1), the formation of the MZ relies on the initial growth of transient alumina which has a higher growth rate than the subsequently growing α -alumina. Kinetic barriers have to be overcome before the transformation of transient alumina polymorphs into stable α -alumina phase can occur. This process takes time. However, the high Cr containing MZ may readily precipitate a stable chromia nucleus which is isomorphic with α -alumina. Chromia acts as a nucleating agent that catalyzes the formation as well as the growth rate of the solid-solution α -alumina at high temperatures [25]. This assumption has experimentally been supported by Bye and Simpkin [26]. The experiments of these authors are based on pyrogenic γ -alumina containing Cr^{3+} and Cr^{6+} . With increasing Cr^{6+} levels, a slowing down of the solution reaction was observed, while it was found to accelerate in a reducing atmosphere. Both results can be assigned to certain oxygen potentials, which indicate an accelerating effect on the α -alumina formation rate at decreasing p_{O_2} . Two-step sintering followed by shear processes or diffusion related nucleation and growth process are discussed as possible mechanisms of the reaction.

In comparison to static laboratory experiments at atmospheres cited, the actual experiments refer to the formation kinetics of the MZ layer on an alumina-forming alloy below a zirconia vapor deposition cloud *in statu nascenti*. The growth process of the MZ ends as soon as the columnar alumina zone (CAZ, compare with Fig. 1) starts growing. The oxygen pressure at the essential CAZ/MZ interface at this time is 10^{-24} atm at 1100°C . The severely decreased p_{O_2} suggests an extremely rapid transformation rate of transient to stable alumina. The final form of the MZ is five times thinner on the Y-devoid substrate, and accordingly the final thickness of the MZ has been reached faster than on Y-containing alloys. The data suggest an

exceptional phase reaction control by diffusion. A likely explanation is given in more detail in the following chapter considering the Hedvall effect.

4.3.2 The effect of Cr content on FCT lifetime

FCT lifetime refers to the gap of more than two orders of magnitude in lifetime when comparing the cyclic and isothermal furnace test results with each other. Generally speaking, the acceleration of a solid-state reaction can often be explained as a consequence of the decomposition of a well-ordered lattice of an ionically bound chemical compound into a transient disorganized lattice state resulting in a condition of an extremely rapid random solid state diffusion of matter. The effect of transient lattice restructuring due to the increased reactivity of a solid during or as a result of a phase transformation has been recognized first about a hundred years ago by Arvid Hedvall [27]. The so-called “Hedvall effect” plausibly results in the apparent destruction of the sesquioxide $(\text{Al,Cr})_2\text{O}_3$ in the MZ into separate Al-rich α_1 and Cr-rich α_2 phases on FCT. While this oxide phase remains still a homogeneous stable $\alpha\text{-(Al}_{0.42}\text{Cr}_{0.58})_2\text{O}_3$ phase on isothermal heating at 1100 °C, the oxide phase net composition of the FCT sample plots right into the miscibility gap of the alumina-chromia system upon cooling [28–30], thereby decomposing into a fine-grained matrix built by the isomorphic Al-rich α_1 and Cr-rich α_2 phases. Both phases are participating in thermodynamic equilibria with some more phases of the MZ. These are imagined to be $\alpha_1 + c\text{-ZrO}_2 + \text{Y}_2\text{Al}_5\text{O}_{12}$ having a garnet structure on one side [31] and $\alpha_2 + c'\text{-ZrO}_2 + \text{YCrO}_3$ having a perovskite structure on the other side [32]. When reheating, the processes will be reversed. As a result, the aging rate in the TBC system and the related diffusivities are accelerated considerably by the cyclic chaotic transient states of concurrent phase decomposition and restoration processes. Likewise, the TBC failure processes are accelerated by the cyclic heating and cooling activity.

At this point of the discussion cyclic furnace test results of a Y-doped non-standard TBC system may add an important aspect. An IN100 substrate having a super finish by centerless grinding got an atypical NiCoCrAlY bond coat with a Cr content of 30 wt%. The TBC system showed despite the excellent prior mechanical preparation of the substrate surface a drastic decrease in FCT lifetime by about 50%. Final failure occurred after 280 hot hours at 1100 °C compared to 550 h for the related standard TBC systems [20]. The Cr content in the MZ was only marginally higher than the comparison values after 417 hot hours. The decrease in the FCT lifetimes of TBC systems as a result of increasing additions of Cr in the bond coat surrogates has been confirmed experimentally in a similar way by Pint and Wright [33]. So the different cation mobility of Al^{3+} and Cr^{3+}

in the $\alpha\text{-Al}_2\text{O}_3$ lattice of the TGO is likely to account for the shorter lifetimes.

The differences in MZ thickness, Cr content in the MZ and FCT service life, the latter by a factor of 5 or 2 to 3 orders of magnitude cannot be explained by the different Cr contents between the NiCoCrAlY bond coats and the DS NiCrAl surrogate. There must be a fundamental distinction between the systems, which can primarily be based on the TGO itself. In both cases, TBC deposition and subjection to FCT produce a TGO at up to 1100 °C, which is based on single-phase $\alpha\text{-(Al,Cr)}_2\text{O}_3$. Upon cool-down, it enters in both cases the two-phase region of the miscibility gap Al-rich α_1 and Cr-rich α_2 , so that three phases coexist next to each other within a transient temperature interval. In the case of the NiCoCrAlY bond coat systems, this interval can expand considerably due to the inclusion of Y as an additional component in the phase assembly. However, in the case of the DS NiCrAl surrogate, in which the net composition of the TGO for the related miscibility gap plots most likely in the central part of the binary $\text{Al}_2\text{O}_3\text{--Cr}_2\text{O}_3$ system and therefore close to the top of the miscibility gap, stricter regulations apply there. The single-phase $\alpha\text{-(Al,Cr)}_2\text{O}_3$ solid solution region borders directly on the $\alpha_1 + \alpha_2$ two-phase region. In this case the Gibbs' phase rule is mandatory which requires an invariant solid state reaction instead of an interval. It is linked to a definite transition point of temperature. The transit is most likely achieved via the Hedvall effect.

High Cr-alloyed BC compositions in TBC systems are apparently a critical issue for cyclic use such as in jet engines. However, if the BCs are needed for a single flight use only, e.g. in particular LH/LO-powered rocket combustion chambers made of precipitation-hardened Cu alloys, then the use of Cr-based alumina forming NiCoCrAlY-type BCs optimized for compatibility with Cu-base substrates may be useful [34].

4.4 The effect of doping with Y (the “rare-earth element effect”)

4.4.1 Parabolic oxidation rate constants of un-doped/ Y-doped Ni–Al versus p_{O_2}

The group of rare-earth elements (yttrium, scandium, lanthanides) display similar chemical properties. So they introduce similar beneficial effects on the oxidation of alumina-forming (and chromia-forming) alloys and bond coats as well as on the high-temperature stabilization of the tetragonal ZrO_2 phase in TBCs (e.g. CeSZ TBCs [18]). The advantageous decrease in the parabolic oxidation rate constant of alloys through doping, both with the rare-earth element Y and with other reactive elements Zr and Hf, is referred to in summary by the term “reactive element effect”. The main task of the TGO is to increase

the adhesive strength between the substrate alloy and the TGO. The mechanism by which oxidation is controlled by the reactive elements is, however unclear [35].

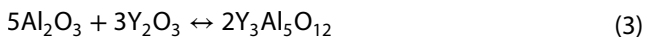
In this study a novel attempt has been employed to explain the reactive element effect by means of a thermodynamic methodology (via point defect thermodynamics in semiconducting oxide lattices of the TGO) [16, 18], as outlined in the following.

The basis for explaining the RE effect focuses on a mechanism that controls the mass transport in the semiconducting lattice of α -Al₂O₃ [36]. One of the rules for defect reactions in stoichiometric ionic compounds is the preservation of the regular site ratio which also applies to α -Al₂O₃. It consists exclusively of cations M_{Al} and cation vacancies V_{Al} and anions X_O and anion vacancies V_O. The site ratio is always

$$(M_{Al} + V_{Al}''') : (X_O + V_O'') = 2 : 3.$$

There are no interstitial positions, no electrons or electron holes and no foreign cations of any other valence. The anion and cation vacancies are the dominant point defects that are characteristic of the Schottky-type of thermal disorder. Their concentration is directly proportional to the extent of the mass transport charges.

The extent of ion disorder depends on the activities of both components; the particular activity of the oxygen component is identical to p_{O_2} . Less disorder in the lattice *alias* less mass transport can be realized by doping the substrate alloy with an element that has a lower dissociation pressure p_{O_2} than alumina has. The dissociation pressure of α -Al₂O₃ at 1100 °C is about 10⁻²⁶ atm [28] is higher than the dissociation pressure of Y₂O₃ of about 10⁻³⁷ atm [37]. The Y dopant reacts immediately with alumina to YAG (Al₅Y₃O₁₂) according



The YAG phase will achieve an intermediate dissociation pressure p_{O_2} between that of alumina (10⁻²⁶ atm) and hafnia (10⁻³⁷ atm) of about 10⁻²⁸ atm [38]. Conversely, this means that at oxygen pressures below 10⁻²⁸ atm, the YAG phase should convert back to alumina and yttria at the expense of the stability of the YAG compound. In other words, the reaction in Eq. (3) runs from right to left given strongly reducing conditions. An analogous case was observed in the TGO of an IN100 sample: the low vanadium content of the substrate served as an indicator for the precipitation of the YVO₄ compound within a defined oxygen potential range in the TGO; below this p_{O_2} range, the compound proved to be unstable [8, 16].

The oxygen pressure dependency of the parabolic oxidation rate constants *alias* of the point defect concentration of V_{Al}''' referring to cation-dominated mass

transport in three-charged compounds like α -Al₂O₃ follows

$$\partial \log [V_{Al}'''] / \partial \log p_{O_2} = 3/16. \quad (4)$$

In a subsequent, even deeper low p_{O_2} regime anion vacancies V_O'' will be governing the oxidation processes. The oxygen pressure dependency of the parabolic oxidation rate constants *alias* of the point defect concentration of V_O'' for anion-dominated mass transport follows

$$\partial \log [V_O''] / \partial \log p_{O_2} = -1/6. \quad (5)$$

Notably the oxides of the 4th group elements hafnia and zirconia do not form compounds nor solid solutions with alumina, however, a certain solubility of oxygen in doped Ni alloys is possible. Their oxygen potential remains unaffected by the higher oxygen potential of alumina. They will probably have an effect on the diffusion processes in the TGO at p_{O_2} pressures below those of the decomposition pressure of YAG of 10⁻²⁸ atm. Consequently the pressure for hafnia can be assumed to be ~ 10⁻³⁷ bar and that of zirconia between those of hafnia and YAG according to 10⁻³⁷ atm < $p_{O_2, zirconia}$ < 10⁻²⁸ atm at approximately 10⁻²⁹ atm.

The related oxidation rate constants of binary Ni–Al compositions of γ and β phase and for Y-doped Ni–Al alloys in Fig. 2 focus on the **reactive element effect**. It satisfies the beneficial RE effect << reducing the scale growth rate >> as mentioned in the introduction. It shows the high degree of correlation between the cited experimental oxidation rates and cataloged oxygen pressures in the TGOs for 1100 °C and the oxygen pressure dependency that has been theoretically created by using point defect thermodynamics.

The oxidation rate constants for Zr- and Hf-doped NiAl have been included in Fig. 2 in anticipation of subsequent discussions of the corresponding experiments including Hf-alloyed substrates and bond coats and literature references. The data of the parabolic oxidation-rate constants are taken from literature. In cases of doubt, the lowest possible RE values were used to counteract the weight-gain rate accelerating effect of over-doping.

To be noted in parenthesis: The comparatively higher parabolic oxidation rate constant for DS NiCrAl has been included as well in Fig. 2. The increased value is not attributed to p_{O_2} , but rather to differences in cation mobility of Al³⁺ and Cr³⁺ as discussed above. The exceptional high weight gain rate constant for the NiAl + Zr alloy compared to the neighboring NiAl + Y alloy is due to additional weight gain as a result of oxygen intake in the Zr-doped NiAl metal matrix. It is therefore reasonable to assume that the decisive rate in thickness growth of Zr-doped NiAl is lower than that of the neighboring Y-doped NiAl. The weight of the scale is reported to be about one tenth of

the total oxidative weight gain [42]. It is also worth considering whether the internal uptake of oxygen in the Zr-doped NiAl substrate is favored under cation-dominated transport conditions, whereas it is slowed down or suppressed under an oxygen-dominated transport mode.

The effect of doping with rare earth elements is reported to lower the oxidation rates corresponding to a factor of 2 to 4 [43]. On the other hand, the doping with the reactive element Hf of the 4th group of the periodic table of elements is reported to result in a ten-fold reduction in the parabolic oxidation rate constant [44].

The issue of « promoting the selective oxidation of Al » as another beneficial RE effect as listed in the introduction is problematic to answer. Kinetic effects are in conflict with the thermodynamic requirements. Before a stable α -Al₂O₃ layer has formed, unstable γ -, δ -, θ - and Al spinel phases have to be passed through. If additional reactive elements are introduced into this phase mixture, the process of phase transformation in the sense of a “phase adjustment” towards the stable oxide can take quite longer [45]. For the successful application of the REE, however, the formation of α -Al₂O₃ is crucial because of the exclusive unique feature of a Schottky-type oxide which satisfies stringent thermodynamic point-defect calculations. If, for example, an approximately 8 μ m thick Al₂O₃ layer has been formed in the final state of a TBC sample after more than 1000 hot hours cycle-tested at 1100 °C (see Fig. 1), the selective oxidation of Al was in the long run promoted due to a reactive element. As this chapter shows, the cause of the positive effect lies in the persistent reduction of the oxygen potential by RE, which prevents the formation of undesired oxides, which are only formed at a higher p_{O_2} . This low p_{O_2} environment likewise stabilizes the adhesion of TBC systems. Thus the beneficial RE effect « improving the scale adhesion » also applies to the given statement.

4.4.2 Failure mode of NiCoCrAlY bond-coated TBC systems

The standard EBPVD TBC systems fail at end of life owing to Al and Y depletion below the TGO and accumulation of Ni, Co, Cr in the TGO, which are going to cause the formation of spinel phases below the TGO. The TGO is a two-phase layer consisting of α -alumina matrix with YAG precipitates, which typically form both peg-like structures at the Me/TGO interface and stringer-like shapes along off-plane grain boundaries (see Fig. 1). Spinel phase emergence at Me/TGO initiates separation failure and spallation of the TBC at the end of life due to inapt p_{O_2} potentials between spinel and metal phase.

During lifetime, Y and Zr accumulate in the alumina matrix of the MZ. While the Zr enrichment is being fed from the YSZ topcoat, the supply of Y is primarily attributable to

the Y reservoir of the metallic bond coat. The transport of the Y³⁺ proceeds via cation vacancies V_{Al}''' in the alumina lattice, the Y³⁺ flow rate is proportional to the concentration of V_{Al}''' . Upon reaching a threshold concentration for Y and Zr in the MZ, the oxygen potential at the Me/TGO interface rises simultaneously to a value that most likely attains the dissociation pressure of alumina. As the p_{O_2} pressure increases further, detrimental spinel phase can be formed. This will make the adhesion along the Me/TGO interface problematical and separation failure will become likely. A certain total amount of Y and Zr represents a life-predicting parameter for EBPVD TBC systems (see Fig. 3) as specified in the following.

Consistent with manifold experimental results on PS NiCoCrAlY bond-coated TBC systems Mumm and Evans [13] stated that scale adhesion on the alternative type of EBPVD bond-coated TBC systems is limited likewise by Me/TGO separation failure due to morphological imperfections at the interface. The authors have based their studies on the TBC system PWA 1484/EBPVD NiCoCrAlY/EBPVD YSZ. However, the authors reported on separation failure in and near the Me/TGO interface due to imperfections and mechanical obstacles around embedded Y₂O₃ particles. However, it has to be kept in mind, that with 0.3 wt% Y the NiCoCrAlY bond coat cited is over-doped by twice the recommended amount for EBPVD bond layers. As a result selective oxidation of Y gives rise to long-term stable yttria inclusions at the decisive Me/TGO interface. Therefore, the authors [13] favor a mechanical cause of failure as opposed to a thermodynamic approach.

In this context it is worth mentioning that a high Y content of 0.35 wt% in the MCrAlY substrate of the present study bond-coated with standard EBPVD NiCoCrAlY shows a positive influence on the failure mode and on service life. The service life is estimated to be at least twice as long. The statement given here is in line with FCT experiments

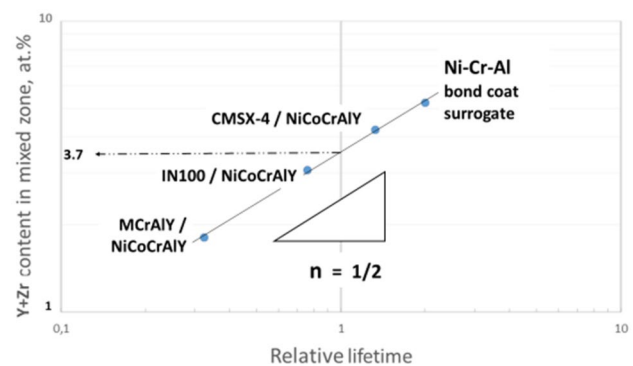


Fig. 3 Y + Zr content in at% in the MZ versus relative lifetime on three different EBPVD NiCoCrAlY bond-coated TBC systems and an undoped NiCrAl bond coat surrogate TBC system in log–log format. 100% of lifetime correlate with 3.7 at% Y + Zr in the MZ [16]

on a PtAl diffusion bond-coated SX superalloy TBC system saying that the finite dopant content in TBC systems needs to be considered when setting up coating lifetime models [45]. For example the Y enriched substrate of the MCrAlY substrate probably provides an internal reserve of reactive elements available in the substrate to ensure a controlled low oxygen potential over an additional period of lifetime.

4.4.3 The effect of the substrate alloys on the performance of NiCoCrAlY bond-coated TBC systems

Limited experimental evidence suggests that the composition and the microstructure of the base alloys have a dramatic effect on TBC lifetime. A particular paper focuses on the effect of the different alloy compositions and structures of the compositions in view of their coat-ability and environmental performance [46]. The oxidation performance of a commercial TBC system on René N5 is compared with NiAl doped with Zr, Hf and Pt [47]; large amounts of elements like Co, Ta, Ti, Hf, Re that readily diffuse from the René N5 substrate to the bond coat and scale are assumed to generate detrimental stresses in the scale affecting scale adhesion. Another study compares the FCT lifetime data of six EB-PVD covered substrate alloys with each other; the high refractory element content of SX alloys is considered the decisive factor for inferior lifetimes. One of the base alloys containing only one refractory element (Mo) proved successful for a base line system [48]. A subsequent paper followed a similar rationale. The FCT lifetimes of various standard EB-PVD bond-coated TBC systems were compared to the content of Y and showed a scatter of the results towards shorter lifetimes. However, if both the real lifetimes achieved for the respective TBC systems and the associated content of Zr in the MZ were also taken into account a square root relationship between “relative lifespan” and Y + Zr mixed zone content for NiCoCrAlY bond-coated/YSZ top-coated systems is attained [15]. The “uniform lifetime relationship” includes Y-free surrogate substrate TBC systems [16] as presented in Fig. 3.

The square root relationship is addressing the effects of an unspecified diffusive transport probably following the base alloy through the bond coat and the TGO up to the MZ. The composition of Y + Zr in the alumina matrix corresponds to the compatibility phase triangle ZrO_2 –YAG ($Y_3Al_5O_{12}$)– Al_2O_3 in the MZ. This variability contradicts the strict requirements for equilibrium conditions of valences that should also hold when applying point defect thermodynamics in Schottky-type three-charged semiconducting oxide lattices of the alumina matrix. The incorporation of tetravalent Zr in the trivalent cation oxide TGO would significantly increase the concentration of cation vacancies. This would result in higher oxidation rates and question the validity of the lifetime relationship. But this case

is excluded, as instead, it appears that a lower state of Zr exists. In modeling the binary Zr–O diagram the combination of the species Zr^{2+} and Zr^{4+} reportedly proved best to obtain consistent thermodynamic data [49]. In this sense, it seems reasonable to have a “joined” zirconia component of hypothetical $ZrO_{1.5}$ alias trivalent Zr that exhibits the same valence state as Al in order to meet the lifetime relationship of Fig. 3. So the total value of Y + Zr represents a single “isovalence value” for two trivalent cations. The end of life thus corresponds to a fixed Me^{3+} content.

Reactive elements in the bond-coated samples like Y and Hf supposedly results primarily from the bond coat and Zr from the YSZ topcoat. They reportedly segregate to the Me/TGO interface and to the grain boundaries in the MZ [50] during the growth of the TGO co-segregating with some minor Al cations [45]. Segregation of tetravalent elements like Si, Hf, Zr and of Ti at grain boundaries and dislocations and back-migrated Zr at the Me/TGO interface were identified via atom probe tomography [51]. Segregation and migration of Ta and Re [40] at grain boundaries was evidenced via transmission electron microscopy [45]. Since the detection of the traces of refractory elements Re and Ta in the TGO presumably succeeded with great experimental effort, the principle of *pars per toto* should apply to all refractory elements still undetected within the TGO.

Point defect reactions in the lattice running at the bond coat side of the TGO most likely exert an effect on the defect concentration towards the exterior TGO including the alumina matrix of the MZ. Any increase in point defect concentration is balanced by the accumulation of reactive elements Y + Zr in the MZ matching to thermodynamic equilibrium conditions.

In order to demonstrate the dynamics of the relationship between refractory element content in the substrate versus the Y + Zr content in the MZ, the refractory element content of the first three substrates of Table 7—given as square root values—are highlighted in Fig. 5 as a function of the Y + Zr content in the MZ of same substrate alloys. Although the cation vacancies are intended for the diffusion of trivalent cation like Al^{3+} and Y^{3+} , as suggested in Eq. (4), they can also be used for the transport of the exclusively tetravalent refractory elements. For reasons of electro-neutrality, however, additional vacancies in the cation sub-lattice must be created. The higher the cation concentration of refractory elements in the TGO, the higher the concentration of cation vacancies required. The diffusion rate of refractory elements in the TGO rises in proportion to the increasing concentration of cation vacancies.

The linear graph in Fig. 5 confirms a square root relationship between Y + Zr content (The total sum represents an isovalence value of these two cations as mentioned before) in the MZs after 417 hot hours and the refractory element content in at% in the substrates; it thus gives an

Table 7 Substrate alloys of this study and their content of the refractory elements Mo, Re, Ta, and W respectively is given as the total sum in at%

Substrate alloy	Total content in at% of refractory elements Mo, Re, Ta, W
IN 100	1.3 at%
CMSX-4	5.5 at%
MCrAlY	0 at%
René 142	4.74 at%
MAR M 002	1.35 at%

indirect evidence for the action of diffusion-controlled processes running between the substrate alloys and the MZ. The service life of TBCs becomes shorter, as the content of refractory alloys in the substrates increases. This particular substrate effect can be described more specifically as the **refractory element effect**.

4.5 The effect of doping with elements of the 4th group, especially Hf

4.5.1 Parabolic oxidation rate constants and their activation energies of Zr- or Hf-doped NiAl

The parabolic oxidation rate constants of alumina forming alloys via grain boundary diffusion of anions and cations in the TGO is controlled by the oxygen potential gradient Δp_{O_2} and the reaction Eq. (5) as well. By the way the mobility of the respective ions, which are subjected to thermally activated jump processes, is crucial for the dominating type of cation or anion transport. The mass transport is typically dominated by one of the two types of ions within a wide p_{O_2} range, where the dominant type of ion transport is dependent on a critical threshold of oxygen pressure at the Me/TGO interface. The oxygen pressure level is decisively determined through the reactive element involved. The type of disorder of the majority of the ion vacancies determines, over a certain p_{O_2} range, the p_{O_2} dependence for the dominant ion defect concentration. The p_{O_2} dependences for anion or cation dominated transport are given in the Eqs. (4) and (5); their hypothetical ranges are indicated by dotted lines in Fig. 2.

Cation and anion diffusion coefficients depend on the ratio of the mobility of the primary point defects. They jointly determine the extent of thermal activation. Thus the dominant type of ion transport can be attributed to characteristic activation energies for oxidation which are indicative of any diffusion-related processes the lifetimes of EBPVD TBC systems included. E.g. the activation energy

of lifetime for the IN100/NiCoCrAlY/YSZ system is reportedly 358 kJ mol^{-1} [15].

Figure 4 clearly reveals two different kinetics and activation energies of oxidation as a function of the doping with Zr or Hf. Oxidation is a result of inward-dominated mass transport in the case of the Zr-doped alloys, as also observed for Y-doped alumina formers. Y and Zr doped alloys show about the same activation energies of oxidation. In contrast the mass transport for the Hf-doped alloys requires a higher activation energy. This mass transport

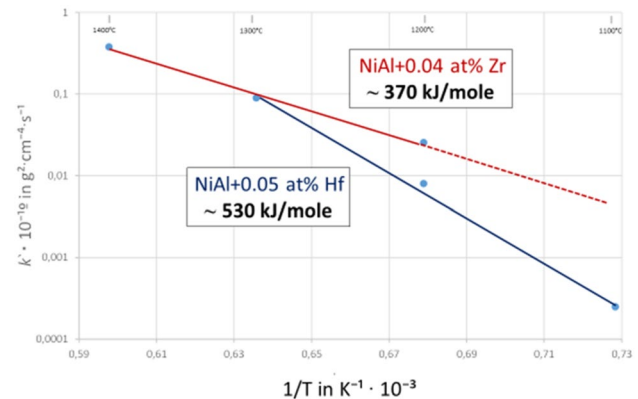


Fig. 4 Arrhenius graph, showing the parabolic oxidation rate constants k' for 0.04 at% Zr-doped NiAl at 1200 to 1400 °C (average of two measurements) [40] and 0.05 at% Hf-doped NiAl (values for 1100 to 1200 °C) [41]. They deliver the appropriate activation energies for the transport of matter of roughly 370 kJ/mole in the actual Schottky-type crystal lattices of α -alumina representing **cation-dominated** transport via point defects of Al vacancies V_{Al}''' for Zr-doped NiAl and the higher activation energy of about 530 kJ/mole assigned to **anion-dominated** mass flow via oxygen vacancies V_O for 0.05 at% Hf-doped NiAl

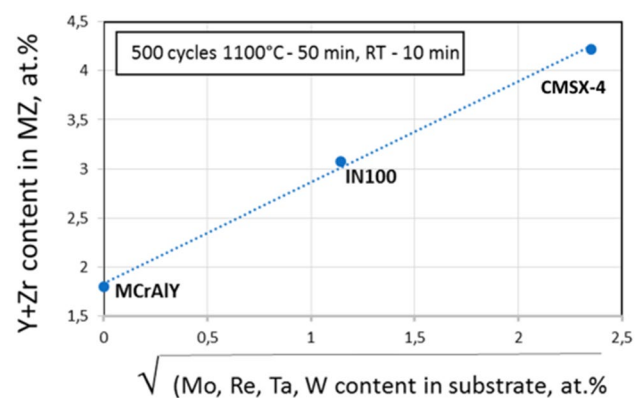


Fig. 5 Refractory element content (square root values) of YSZ top-coated Ni-base alloy versus Y+Zr content in the MZ after exposure to identical hot hours (417 h at 1100 °C). The straight line representing a square root relationship indicates outward diffusion controlled transport of the refractory elements in dependence of the Y+Zr content in the MZ, in which the increasing Y+Zr concentration increases in proportion to the cation vacancy concentration

obviously has culminated in an outward-dominated mass transport by assistance of oxygen vacancies.

A noticeable influence of the dopants Zr- and Hf on the outward flux is reported: replacing Zr with Hf reduces the outward flux by a factor of 5 to 10 in NiAl [50]. Hence a different performance e.g. in the lifetime via FCT of Zr or Hf doped TBC systems is likely.

The “uniform lifetime relationship” in Fig. 3 and the refractory element effect equation of Fig. 5 both show a square root parabolic relationship to the Y + Zr content in the MZ for cation-controlled TBC systems. They document the close interrelationship between

- the refractory element content (Mo, Re, Ta, W) in the substrate alloy,
- the total content of the two reactive elements Y and Zr in the mixed zone, with the total sum of these cations basically representing a Me^{3+} isovalence value,
- the relative lifetime in % of the EBPVD TBC system.

These three issues, namely the alloy specifications, the chemical composition of the mixed zone and a “relative time specification”, which is decisive for kinetic processes, are interrelated and linked in a control loop that determines the service life and adhesion of cation-ruled TBC layer systems within a certain composition range for Y + Zr in the mixed zone.

The growth rate of TGO below the MZ layer of TBC systems, on the other hand, fits to a sub-parabolic relationship according $k_p \sim t^{0.33}$ [48] which is independent of the parameters listed above. So a hypothetical statement of a critical TGO thickness is questionable.

4.5.2 FCT performance of Zr or Hf doped TBC systems

In this chapter, PVD related FCT experiments on TBC systems having a magnetron-sputtered bond coat doped with either Zr or Hf have been carried out by Saldaña, Schulz, Mondragón Rodríguez, Caceres-Diaz, and Lau. They are referred to in [52]. The magnetron-sputtered bond coats are Ni—36 Al—11Cr—0.8 X in at% with X being Zr or Hf. The substrates are IN100 and CMSX-4. The cycles to failure are given in Fig. 6.

The FCT results of the Zr-doped samples of [52] in Fig. 6 apparently confirm the statement previously made for Y-doped samples in this study: the service life of TBCs becomes shorter, as the content of refractory elements in the substrates IN100 and CMSX-4 increases as to 1.3 → 5.5 at%. The FCT results on the Hf-doped samples, however, show an inverse relationship of the lifetimes to their substrates which differ noticeably. However, the lifespan should not differ significantly due to different refractory element contents if dominant anion transport

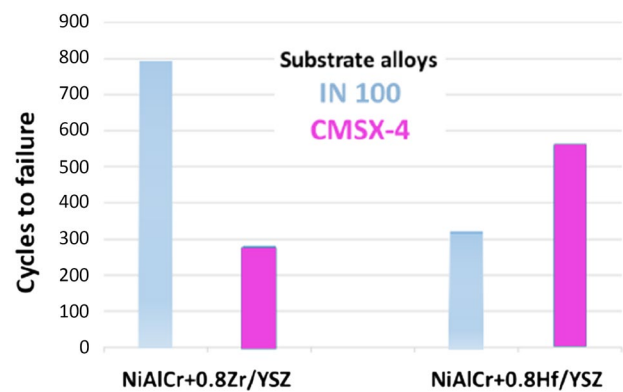


Fig. 6 Cycles to failure on FCT at 1100 °C of TBC systems having magnetron-sputtered Zr-doped bond coats (left side) and analogous Hf-doped bond coats (right side) on IN100 and CMSX-4 substrates (courtesy U. Schulz). The compositions of the bond coats are Ni—36 Al—11Cr—0.8 X in at%, X being Zr or Hf

for both Hf-doped samples is assumed. In addition, the formation of spinel phase at the Me/TGO interface of the IN100 sample is mentioned which is indicative for cation-dominated diffusion processes. These contradictions will be taken into account.

4.5.3 FCT performance of Hf-containing superalloy samples having NiCoCrAlY bond coats versus CMSX-4 employing a Hf-modified bond coat

The Hf-rich superalloys René 142 and MarM002 being coated with standard NiCoCrAlY EBPVD TBC system have been subjected to extensive standard FCT—for 1695 and 935 hot hours—without any foreseeable end-of-life. The determination of the lifetimes was therefore suspended for internal capacity reasons. In parallel to these FCT experiments, more detailed tests, which also refer to longer FCT operating times, were carried out on CMSX-4 NiCoCrAlYHf bond-coated samples. An average lifetime of 4550 hot hours was determined. The FCT performance observed on the Hf-rich superalloy samples, which have a significantly differing content of refractory elements of 4.74 and 1.35 at%, is even so uniform (see Table 7). This observation even applies to all three sample variants, which have fundamental similarities within the set time frame. Thus, based on the same performance, the three sample variants are taken as representative for each other in the following with the focus on the Hf-modified variant. Considering an extensive FCT lifespan for the three sample variants and the related supposed equivalent activation energy of lifetime of 474 kJ mol^{-1} indicative of anion-ruled transport processes a hypothetical uniform lifetime of 4550 h is assumed.

A typical cross-sectional view given in Fig. 7 represents the phase formations in the TGO on an Hf-modified bond

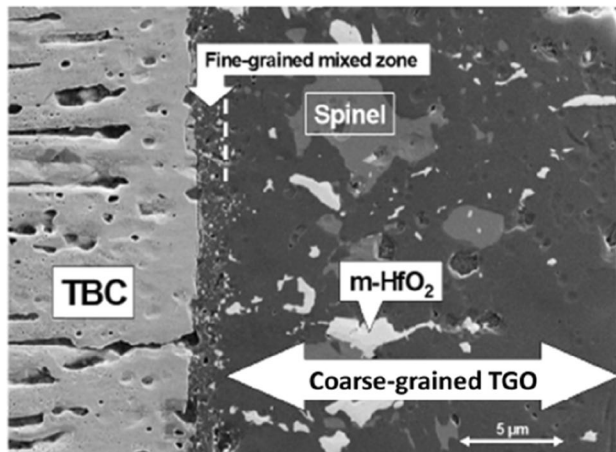


Fig. 7 Cross section through the TBC/TGO zones of a CMSX-4/NiCoCrAlYHf/YSZ TBC system at intermediate life (3104 cycles at 1100 °C). It details the TGO being defined by a fine-grained MZ next to the YSZ topcoat and a coarse-grained TGO at the right. The NiCoCrAlYHf bond coat (not shown here) is co-doped with 0.18 at% Hf

coat at intermediate life. The fine-grained MZ shows similar in size and microstructure to the “standard” MZ on NiCoCrAlY bond coats having no Hf. However a multi-phase coarse-grained MZ is established instead of an adjacent single-phase CAZ. Imbedded hafnia and spinel phases can be easily distinguished from each other due to their light and medium gray tint. They stand out clearly from the dark gray background of the alumina matrix.

The adhesion between the standard t'-zirconia phase of the TBC and in the Hf-containing fine-grained MZ is inferior, as indicated by the nucleation of a crack along the TBC/fine-grained MZ interface (see white arrow) in Fig. 8. The main cause of this rejection reaction between fine-grained MZ and YSZ TBC is presumably related to the reduced content of t'-stabilizing Y. While in comparison the Y content in the MZ of standard coated samples in their intermediate life is 0.5 to 1 at% Y, it has decreased by about an order of magnitude within the Hf-modified fine-grained MZs.

When comparing the phase ratios in the coarse-grained MZ of imbedded spinel phases and hafnia in the intermediate and final state of life they imply that the growth rate of the inclusions slows down or stops in the course of FCT while the growth of the alumina matrix phase keeps going. However, this growth does not follow a sub-parabolic rate relationship [48], but rather an approximate TGO growth behavior somewhere between a parabolic and linear increase in thickness with time. The indicated dynamics, both chemical and morphological, certainly play an important role in TBC failure, but do not provide any well-defined information within this study.

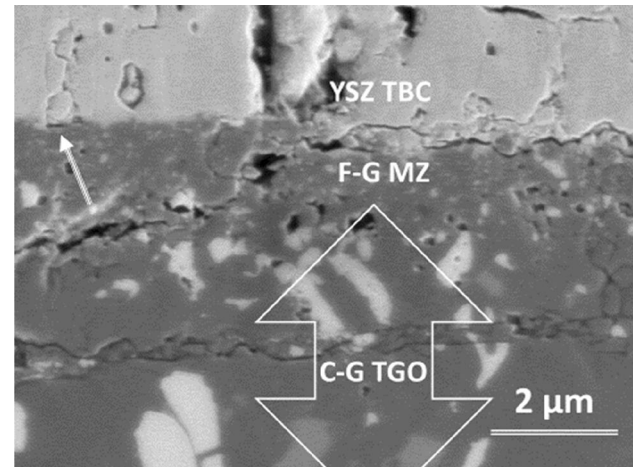


Fig. 8 Cross section through the intermediate part of a TBC system showing the onset of YSZ TBC/TGO failure of a Y + Hf co-doped TBC system with 0.18 at% Hf of CMSX-4/NiCoCrAlYSiHf/YSZ at intermediate life after 1584 cycles at 1100 °C (1320 h at 1100 °C). The kick off of a separation crack (indicated by the white arrowhead at the upper left side) at the F-G MZ (fine-grained MZ)/YSZ TBC interface suggests the nucleation of an incompatibility reaction between the YSZ zirconia phase of the TBC and the MZ. Simultaneous cracking proceeds along the fine-grained MZ/YSZ TBC interface at the right and in the C-G TGO (coarse-grained TGO) close below the F-G MZ

Figures 9 and 10 show cross-sectional views comparing two extreme failure-at-the-end-of-life scenarios, displaying different fracture appearances, which in both cases were caused by mechanically weak and brittle spinel and hafnia phases and/or chemical MZ/YSZ TBC interactions. On close inspection small white-contrasted areas can be occasionally detected up to 5%, which indicate a partial crack deviation from the TGO into the lower part of the TBC. Obviously the individual spread of the cracks seems to be extremely random both within the same sample and from sample to sample. The failure scenarios of the TBC systems reveal a fundamental difference between that of the Hf-doped samples (similarly assumed as hypothesis for René 142 and MarM002) and the typical Me/TGO separation failure mode of the standard NiCoCrAlY bond-coated TBC samples. Therefore a typical crack propagation scheme cannot be predicted for the anion-ruled TBC systems.

The sum of the Y + Zr content in the fine-grained MZ (Y + Zr in at%) is plotted on a logarithmic scale as a function of time, see Fig. 11. An average lifetime of 4550 h is hypothetically established for the Hf + Y co-dope bond-coated TBC system via graphical approximation for RE off-diffusion and is taken as representative for the other Hf-dominated TBC systems. The chemical composition of the MZ of the at-end-of-life scenario has not yet been analyzed because of the disintegrated state of this zone. Therefore, a critical Y + Zr content in the MZ is hypothetically predicted

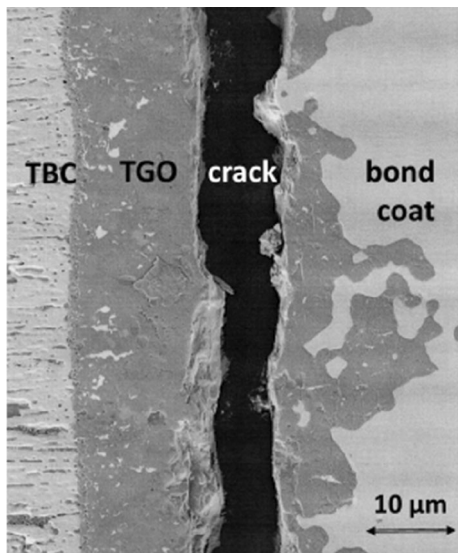


Fig. 9 Separation failure at end of life of Y+Hf co-doped bond-coated TBC system with 0.18 at% Hf on CMSX-4 substrate (6549 cycles at 1100 °C)

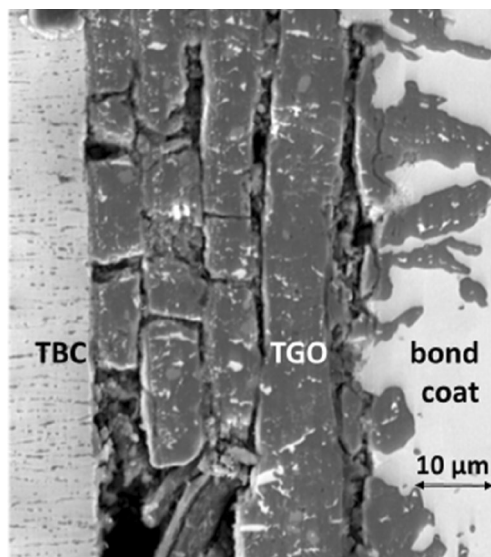


Fig. 10 FCT failure at end of life of Hf+Y co-doped bond-coated TBC system with 0.35 at% Hf on CMSX-4 substrate (1450 cycles at 1150 °C)

instead and set for FCT failure. As a result Fig. 11 represents a “uniform lifetime relationship for anion-controlled TBC systems”. The service life of the TBC systems and the RE contents in the fine-grained MZ that both decrease with the actual lives at temperature are linked: They can be assigned to a common path of Y + Zr contents in the MZ over time at high temperatures, which is ended in an approximately uniform time window due to failure of the thermal protection layer system.

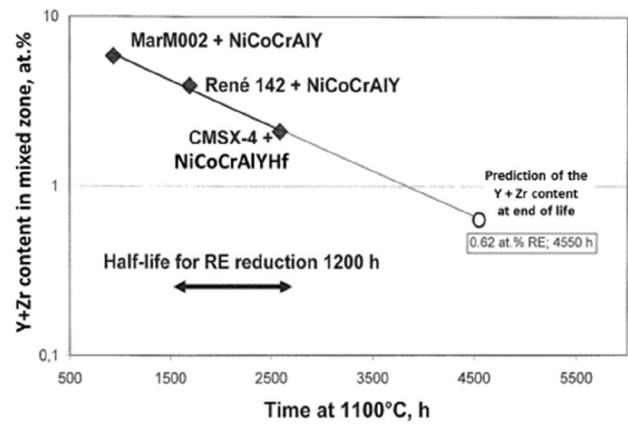


Fig. 11 Y+Zr content (at%) in the fine-grained mixed zone versus time at 1100 °C during FCT of Hf+Y co-doped TBC samples. Notably the provision of the Hf co-dopant stems from the substrate or from the bond coat as well. The half-life value of 1200 h is calculated from the downtilt; it allows to estimate the RE content at FCT failure

The trend of the descending straight line apparently corresponds to the inward-directed RE off-diffusion via predominant oxygen vacancies and oxygen inward diffusion. The reasonable approximation of the data to a straight line suggests a uniform transport mechanism in TBC systems without regard to the different manufacturing routes e.g. via PS or PVD and to diverse refractory alloy compositions of the substrates. Thus the beneficial RE effect related to « changing of the scale growth mechanism from predominantly outward to oxygen inward transport » also applies to the TBC systems having Hf-containing superalloy substrates or Hf-modified bond coats.

4.5.4 FCT performance of IN100 samples having a Hf-modified bond coat

The **IN100 samples** having Y + Hf co-doped bond coats show a comparatively short cyclic life of 760 h (912 cycles) at 1100 °C as shown in Fig. 12. The comparative results obtained on IN100 and on CMSX-4 substrates are analogous to those from magnetron sputter bond-coated TBC systems doped with Hf shown in Fig. 6 [52]. The life of the Y + Hf co-doped bond-coated IN100 sample is close to the comparative lifetime displayed as well by IN100 standard samples with NiCoCrAlY bond coats of 550 h as with like samples having had a preceding 4000 grit super finish of 1185 h. Evidently the basic failure mechanisms are alike. The diffusion processes in the TGO are no longer controlled by anion vacancies but via cation vacancies. Hf is thereby losing its individual reactive element effect.

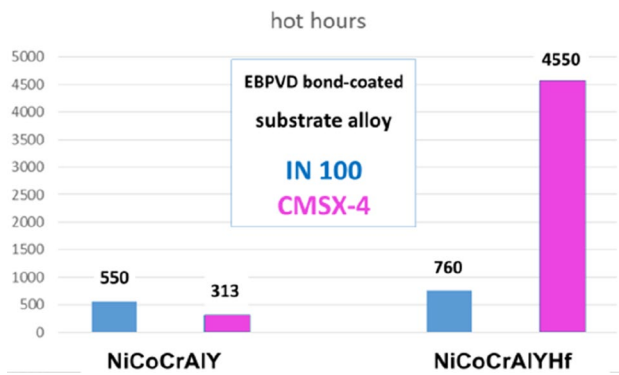


Fig. 12 FCT lifetime in hours at 1100 °C of superalloy substrate based TBC systems having standard NiCoCrAlY bond coats (left) compared to the Hf-modified bond-coated TBC systems (right)

The substrates underlying the Hf-modified bond coats had all been given a super finish via centerless grinding. This pretreatment probably had hardly any effect on the lifespan of the CMSX-4 samples being anion-controlled because the cracks occurred almost exclusively within the TGO and not at the Me/TGO interface. However, the superfinishing obviously had a beneficial effect on the service life of the cation-diffusion controlled IN100-based variant, which had a 38% longer service life of 760 hot hours compared to the standard IN100 samples of 550 hot hours.

In the TGO and bond coat of the Y + Hf co-dope bond-coated TBC system on a CMSX-4 substrate, the oxide phases of Al, Hf and Y should play an essential role. One of the predicted phases next to the growth front Me/TGO is YAG ($Y_3Al_5O_{12}$) according to the ternary system alumina–hafnia–yttria [53]. This phase, however, was not observed in the TGO of TBC systems on **CMSX-4 substrates** described above. In analogy to this system, a similar study on an FCT treated DS solid-solution-strengthened SX superalloy sample with Y + Hf co-doped NiCoCrAlHfY bond coat is cited [54]. In the TGO/bond coat area, nanoscale particles with the net composition $4HfO_2 + Y_2O_3$ with an apparently cubic fluorite structure were determined. YAG phase, however, has not been confirmed in this TBC system either. Presumably further basic research on this problem area is required.

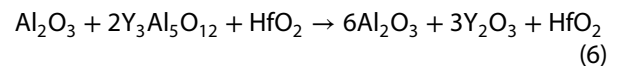
If a corresponding FCT sample of IN100 was used as a substrate, however, YAG was present in the TGO. In order to check the vanadium content in the IN100 substrate as the cause of the different behavior of the TBC systems with IN100 or CMSX-4 substrate alloys, the behavior of a vanadium-free comparison system is considered [55].

At this point of the discussion, two issues need to be clarified.

1. The phase relationships in the TGO on Hf-modified bond-coated **CMSX-4 substrate** will be reinterpreted.

The underlying ternary system [53] is supposedly based on measurements made at atmosphere. Certain stable binary oxide compounds of this ternary system are supposed to be unstable at low oxygen partial pressures $\leq 10^{-27}$ atm at 1100 °C: particularly the formation for YAG phase given in Eq. (3) should convert back to alumina and yttria in order to establish a suitable ternary diagram for the low oxygen pressure range. The formation of alumina, hafnia, yttria and YAG in one stable phase assemblage, possibly with the bond coat, would contradict Gibbs' phase rule. In this case there are too many phases together. The binary HfO_2 - Y_2O_3 system dominating as a purely eutectic system with a eutectic at around 70 mol% Y_2O_3 [55] suggesting that upon cooling decomposition of a $4HfO_2 + Y_2O_3$ bulk composition [54] into the components HfO_2 and Y_2O_3 is most likely.

With these arguments in mind a corrected phase relationship would result from this estimate giving



Equation (6) perfectly matches the fine-grained, multiphase oxide phase assemblage typically retrieved from those microstructures [56]. This hypothetical phase relationship from Eq. (6) has been incorporated in Table 8.

2. The diffusion processes in the TGO on Hf-modified bond-coated **IN100 substrate** are no longer anion-but cation-controlled. The motivation for the reversal of the transport mechanism must be interpreted.

The particularly high Ti content of 5 wt% (= 5.7 at% Ti) in precipitation-hardening IN100 superalloy is five times higher than the Ti content in CMSX-4. Thus the dominant effect of Hf may possibly be undermined by the high Ti content in IN100 and not by the vanadium content of 1 wt%. Related oxidation experiments on a comparison system of Hf doped NiAl bond coats on vanadium-free substrate alloys containing 4.3 at% Ti are reported to show the formation of spinel phase insets either [56]. The results suggest that a high concentration of Ti is a crucial factor to limit the dominant role of Hf and to promote a cation-controlled transport mechanism in alumina.

Obviously, a dual substrate effect dominates the growth mechanism. Depending on their respective concentrations, they determine the type of oxidation via anion or cation control. Although the transition from cation vacancy to anion vacancy patronized mass flow is dependent on p_{O_2} pressure, it is also decisively influenced by the valence state of the diffusion elements Hf and Ti. The valence state of Hf is only tetravalent. The transport of Ti ions in alumina scales, however, may be more enlightening

Table 8 Comparative sequence of phases from outside to inside in FCT TBC systems with Y-doped bond coat (left) and Y + Hf co-doped bond coat (right). Suspected oxygen partial pressures effective at phase boundaries are indicated for 1100 °C as footnote

TBC systems Layer sequence	Y dope bond-coated TBC Phases	Y + Hf co-doped TBC system Phases
TBC topcoat	t' YSZ	t' YSZ
TGO Mixed Zone (fine-grained)	$\alpha\text{-Al}_2\text{O}_3 + \text{t}' \text{YSZ } p_{\text{O}_2}$ at atmospheric pressure	$\alpha\text{-Al}_2\text{O}_3 + (\text{Zr,Hf})\text{O}_2 p_{\text{O}_2}$ at atmospheric pressure
TGO (thermally growing oxide layer)	$\alpha\text{-Al}_2\text{O}_3 + \text{YAG CAZ}$ (columnar alumina zone) $p_{\text{O}_2} \leq 10^{-27}$ atm	$\alpha\text{-Al}_2\text{O}_3 + \text{m-HfO}_2 + \text{spinel } (\text{Ni,Co})(\text{Al,Cr})_2\text{O}_4$ $p_{\text{O}_2} = 10^{-20 \leftrightarrow -27}$ atm (coarse-grained TGO) $\alpha\text{-Al}_2\text{O}_3 + \text{m-HfO}_2 + \text{Y}_2\text{O}_3 p_{\text{O}_2} \leq 10^{-37}$ atm
Bond coat	$\beta\text{-NiAl}$ rich BC	BC + internal m-HfO ₂

by the variable valences of 1 to 4. Ti is reported to diffuse rapidly upward towards the scale/gas interface particularly along grain boundaries of the CAZ (columnar alumina zone) of the TGO [57]. They are present in a much higher concentration compared to the Hf content.

In this context the following site reaction in the lattice is hypothesized. The cation transport in the TGO normally happens via site changes with existing cation vacancies V_{Al}''' , which are intended for the transport of trivalent cations. If, for example, instead of a trivalent cation a monovalent cation Ti^+ enters a vacancy V_{Al}''' , it turns now into a regular one-charged atom site in the cation sub-lattice. However, this arrangement contradicts the electro-neutrality condition with respect to equal amounts of positively and negatively charged point defects. If, on the other hand, an oxygen vacancy V_{O}'' in the anion sub-lattice is removed, then the electro-neutrality condition is satisfied. The given example for a single cation is transferable to similar specific cases of the highly Ti-alloyed IN100 based substrate of the TBC system. Hence a correspondingly high reduction in anion vacancies is expected likewise for other low-charged Ti cations which all result in cation-controlled diffusion processes. The cation-controlled diffusion initiates a different failure mode and a shorter lifetime. An increase in the number of cation vacancies as a result of Ti additions is likewise reported for the oxidation behavior of FeCrAl alloys [58].

5 Conclusions

The cyclic life and failure of EBPVD thermal barrier coating systems on selected Ni-base substrates were tested at 1100 °C. Apart from the main focus of this study, that is the mechanisms of compositional effects related to both the substrate as well as reactive element doping, the surface constitution of substrates is a decisive parameter which must not be overlooked.

A relatively rougher surface of uncoated substrates aroused a locally increased oxygen pressure Δp_{O_2} during the oxidation of the coated samples, which initiates

the premature formation of less-protective interfaces and shorter service life. Therefore the oxygen pressure p_{O_2} at the growth front of scales defines a fundamental key parameter for decoding the mechanisms ruling the lifetime and failure mode of Ni-based thermal barrier coating systems.

Addressing the role of Cr as a typical substrate element, a standard NiCoCrAlY bond coat over-alloyed with additional 10 wt% Cr reduced the service life of the TBC system by 50%. The accelerated transport or aging process is not caused by a higher concentration of cations in the TGO, but rather by the presence of equivalent Cr^{3+} ions, which are far more agile, instead of Al^{3+} ions. Thus, shorter lifetimes of the TBC systems and higher oxide growth rates happen for cation-ruled systems due to higher Cr contents.

Cyclic lifetime data of the TBC systems were recorded and correlated to related chemical compositions in the mixed zone (MZ) of the thermally grown oxide (TGO). The lifetime data and associated chemical data of the MZ showed time-dependent and concentration-dependent mass transport relationships. They could be assigned both to alloy substrate and bond coat elements and their concentrations. These elements exert a specific influence on the oxygen pressure in the TGO and on the associated vacancy concentrations of oxygen and cations. The adhesion of the TGOs to the metal substrates is increased by the action of reactive elements in lowering of the oxygen pressure at the TGO front below the decomposition pressure p_{O_2} of $\alpha\text{-Al}_2\text{O}_3$.

The cation mass transport refers to cation vacancy concentrations. The life-determining transport processes in Schottky-type lattice of α -alumina in the TGO are characterized by means of point defect thermodynamics. So the following statements that are based on indirect evidence obtained by point defect calculations are:

The prevailing experiments being conducted on Ni-base alloys without and with standard Y-containing bond coats and YSZ ceramic thermal barrier topcoats suggest, that an increasing refractory element content in the substrates reduces the TBC lifespan for cation-ruled systems.

The increasing contents of (tetravalent) refractory elements in the substrate alloys that care for additional cation vacancies are directly proportional to the concentration of cation vacancies V_{Al}''' .

The experiments in comparison on Ni-base alloys with no Hf content but with a Hf-modified bond coat as well as on Hf-containing Ni-base alloys with un-modified Y-containing bond coats and both with YSZ ceramic thermal barrier topcoats suggest, that a dominant effect of Hf dopant on ionic transport processes favors oxygen-ruled transport reactions in TBC systems. They tend to approach identical lifetimes since the concentration of oxygen vacancies V_O'' cannot be influenced by any potential anions having a different valence than V_O'' .

A supplementary side experiment on a γ' precipitation-hardened Ni-base alloy with no Hf content (IN100 superalloy) but with a Hf-modified bond coat and with YSZ ceramic thermal barrier topcoat suggests, that anion-ruled transport reactions can be critically affected by an increasing Ti content of the substrates thus favoring cation-ruled transport reactions. The anion-ruled transport reactions via oxygen vacancies V_O'' can be overcome by an oversupply of low-charged cations of corresponding alloying elements creating additional cation vacancies V_{Al}''' in the cation sub-lattice to trigger a conversion to a cation-dominated transport scenario.

Acknowledgements The in-depth discussions with DLR colleague Wolfgang Braue on the general outline of this paper are gratefully acknowledged.

Funding Open Access funding enabled and organized by Projekt DEAL.

Compliance with ethical standards

Conflict of interest The author declares that they have no competing interests.

Open Access This article is licensed under a Creative Commons Attribution 4.0 International License, which permits use, sharing, adaptation, distribution and reproduction in any medium or format, as long as you give appropriate credit to the original author(s) and the source, provide a link to the Creative Commons licence, and indicate if changes were made. The images or other third party material in this article are included in the article's Creative Commons licence, unless indicated otherwise in a credit line to the material. If material is not included in the article's Creative Commons licence and your intended use is not permitted by statutory regulation or exceeds the permitted use, you will need to obtain permission directly from the copyright holder. To view a copy of this licence, visit <http://creativecommons.org/licenses/by/4.0/>.

References

1. Pfeil LB, U.K. Patent No. 459848 (1037)

- Hou PY (2011) The reactive element effect—past, present and future. *Mater Sci Forum* 696:39–44
- Smialek J, Miller R (2018) Revisiting the birth of 7YSZ thermal barrier coatings: Stephan Stecura †. *Coatings* 8:255
- Wagner C (1933) Beitrag zur Theorie des Anlaufvorgangs. *Z Physik Chem* B21:25
- Goward GW (1988) Progress in coatings for gas turbine airfoils. *Surf Coat Technol* 108–109:73–79
- Leyens C, Schulz U, Braue W, Yang YQ (2001) Formation of the alumina-zirconia bonding zone in EB-PVD thermal barrier coatings. In: McNallan M, Opila E (eds) *High temperature corrosion and materials chemistry III, 2001–2012*. The Electrochemical Society, Pennington
- Stiger MJ, Yanar NM, Jackson RW, Laney SJ, Pettit FS, Meier GH, Gandhi AS, Levi CG (2007) Development of intermixed zones of alumina/zirconia in thermal barrier coating systems. *Metall Mater Trans* 38A:848–857
- Braue W (2005) Phase relationships and defect structure during oxide formation and growth in NiCoCrAlY and (Ni,Pt)Al-based TBC systems. In: 2005 Gordon research conference on high-temperature corrosion, July 24–29, 2005, Colby Sawyer College, New London, NH, USA
- Evans AG, He MY, Hutchinson JW (1997) Effect of interface undulations on the thermal fatigue of thin films and scales on metal substrates. *Acta Mater* 45:3543–3554
- Nichols JR, Evans HE, Saunders SRJ (1997) Fracture and spallation of oxides. *Mater High Temp* 14:5–13
- Wright PK, Evans AG (1999) Mechanisms governing the performance of thermal barrier coatings. *Curr Opin Solid State Mater Sci* 4:255–265
- Hutchinson JW, Evans AG (2002) On the delamination of thermal barrier coatings in a thermal gradient. *Surf Coat Technol* 149:179–184
- Mumm DR, Evans AG (2000) On the role of imperfections in the failure of a thermal barrier coating made by electron beam deposition. *Acta Mater* 48:1815–1827
- Stiger MJ, Yanar NM, Topping MG, Pettit FS, Meier GH (1999) Thermal barrier coatings for the 21st century. *Zeitschrift für Metallkunde* 90:1969–1978
- Fritscher K, Braue W, Schulz U (2013) Assessment of cyclic lifetime of NiCoCrAlY/ZrO₂-based TBC systems via reactive element enrichment in the mixed zone of the TGO scale. *Metall Mater Trans* 44A:2070–2082
- Fritscher K, Kröder CJ, Schulz U (2016) Adherence and failure of an EBPVD 7YSZ coating on a β/γ -NiCrAl substrate: a pilot study. *Oxid Met* 86:279–298
- Fritscher K (2003) Eutectic structures in the Ni–Co–Cr–Al system obtained by plasma-spraying and by Bridgman growth. *J Cryst Growth* 250:146–157
- Fritscher K (2019) Life and FCT failure of yttria- and ceria-stabilized EBPVD TBC systems on Ni-base substrates. *Oxid Met* 91:131–157
- Kaden U (2003) Einfluss der Substratlegierung CMSX-4 auf die Lebensdauer eines Wärmedämmschichtsystems, Ph.D. RWTH Aachen
- Schulz U (2002) Communication for optimal EBPVD coating and alloy layer control in the jointly used coater
- German RM (1996) *Sintering theory and practice*. Wiley, Hoboken
- Yang JC, Nadarzynski K, Schumann E, Rühle M (1995) Electron microscopy studies of NiAl/ γ -Al₂O₃ interfaces. *Scr Metall Mater* 33:1043–1048
- Santoro GJ, Deadmore DL, Lowell CE. Oxidation of alloys in nickel-aluminum system with third-element additions of chromium, silicon, and titanium at 1100°C, Lewis Research Center, Cleveland, Ohio, NASA Technical Note D-6414, July 1971, 28 p

24. Bedu-Amissah K, Rickman JM, Chan HM, Harmer MP (2007) Grain-boundary diffusion of Cr in pure and Y-doped alumina. *J Am Ceram Soc* 90:1551–1555
25. Brumm MW, Grabke HJ (1992) The oxidation behaviour of NiAl-I. Phase transformations in the alumina scale during oxidation of NiAl and NiAl-Cr alloys. *Corros Sci* 33:1677–1690
26. Bye GC, Simpkin GT (1974) Influence of Cr and Fe on Formation of α -Al₂O₃ from γ -Al₂O₃. *J Am Ceram Soc* 57:367–371
27. Hedvall JA. Allgemeine Betrachtungen der Umwandlungsreaktivitätseffekte (engl.: On conversion reactivity effects). In: Die Wissenschaft -Einführung in die Festkörperchemie, W. Westphal, F. Viehweg&Sohn, Braunschweig, (1952) Bd.106, 193
28. Saltykov P, Fabrichnaya O, Goczewski J, Aldinger F (2004) Thermodynamic modeling of oxidation of Al-Cr-Ni alloys. *J Alloys Compd* 381:99–113
29. Sitte W (1985) Investigation of the miscibility gap of the system chromia-alumina below 1300 °C. In: Barrel P, Dufour L-C (eds) *Reactivity of solids*. Elsevier, Dijon
30. Besmann TM, Kulkarni NS, Spear KE (2006) Thermochemical analysis and modeling of the Al₂O₃-Cr₂O₃, Cr₂O₃-SiO₂ and Al₂O₃-Cr₂O₃-SiO₂ system relevant to refractories. *J Am Ceram Soc* 89:638–644
31. Lakiza S, Fabrichnaya O, Zinkevich M, Aldinger F (2006) On the phase relations in the ZrO₂-YO_{1.5}-AlO_{1.5} system. *J Alloys Compd* 420:237–245
32. Jayaratna M, Yoshimura M, Somiya S (1984) Subsolidus phase relations in the pseudoternary system ZrO₂-YO_{1.5}-CrO_{1.5} in air. *Am Ceram Soc* 67:C240–C242
33. Pint BA, Wright IG (1995) Cyclic oxidation behavior of cast NiCrAl alloys. In: Opila EJ, McNallan MJ, Chores DA, Hou PY (eds) *High temperature corrosion and materials chemistry*, vol 98-9. The Electrochemical Society, Pennington, pp 263–274
34. Schulz U, Fritscher K, Peters M, Greuel D, Haidn O (2005) Fabrication of TBC-armored rocket combustion chambers by EB-PVD methods and TLP assembling. *Sci Technol Adv Mater* 6:103–110
35. Whittle DP, Stringer J (1980) Improvements of high temperature oxidation resistance by addition of reactive elements or oxide dispersions. *Trans R Soc Lond* 295:309–329
36. Schmalzried H (1981) *Solid state reactions*, 2nd edn. Verlag Chemie, Weinheim
37. Barin I, Knacke O, Kubaschewski O (1977) *Thermochemical properties of inorganic substances*. Springer, Berlin
38. Balmain J, Huntz AM (1996) Improvement of the application of an electrochemical method for the determination of transport properties of an α -alumina scale. Part II: influence of yttrium and palladium on alumina scales developed on a β -NiAl alloy. *Oxid Met* 46:213–234
39. Pint BA, Nagaraj BA, Rosenzweig MA (1996) Evaluation of TBC-coated β -NiAl substrates without a bond coat. In: Dahorte N, Hampikian JM, Stiglich JJ (eds) *Published in high temperature coatings II*. TMS Warrendale, Pittsburgh, pp 163–174
40. Pint BA, Hobbs LW (2004) The oxidation behavior of Y₂O₃-dispersed β -NiAl. *Oxid Met* 61:273–293
41. Stiger MJ, Yanar NM, Topping MG, Pettit FS, Meier GH (1999) Thermal barrier coatings for the 21st century. *Int J Mater Res Adv Tech* 90:1969–1978
42. Barrett CA (1988) Effect of 0.1 at.% zirconium on the cyclic oxidation resistance of β -NiAl. *Oxid Met* 30:361–389
43. Pint BA (2001) Progress in understanding the reactive element effect since the Whittle and Stringer literature review. In: *Proceedings of the J. Stringer symposium*
44. Rybicki GC, Smialek JL (1989) Effect of the θ - α -Al₂O₃ transformation on the oxidation behavior of β -NiAl + Zr. *Oxid Met* 31:275–304
45. Pint BA, More KI (2009) Characterization of alumina interfaces in TBC systems. *J Mater Sci* 44:1676–1686
46. Kimmel J, Mutasim Z, Brentnall W (2000) Effects of alloy composition on the performance of Ytria stabilized Zirconia thermal barrier coatings. *J Eng Gas Turbines Power* 122:393–400
47. Pint BA, Wright IG, Lee WY, Zang Y, Prüßner K, Alexander KB (1998) Substrate and bond coat compositions: factors affecting alumina scale adhesion. *Mater Sci Eng A* 245:201–211
48. Schulz U, Menzebach M, Leyens C, Yang YQ (2001) Influence of substrate material on oxidation behavior and cyclic lifetime of EB-PVD TBC systems. *Surf Coat Technol* 146-147:117–123
49. Wang C, Zinkevich M, Aldinger F (2004) On the thermodynamic modeling of the Zr-O system. *Comput Coupling Phase Diagr Thermochem* 28:281–291
50. Boll T, Unocic KA, Pint BA, Mårtensson A, Stiller K (2017) Grain boundary chemistry and transport through alumina scales in NiAl alloys. *Oxid Met* 88:469–479
51. Chen Y, Reed RC, Marquis EA (2014) Interfacial solute segregation in the thermally grown oxide of thermal barrier coating structures. *Oxid Met* 82:457–467
52. Muñoz Saldaña J, Schulz U, Mondragón Rodríguez GC, Caceres-Diaz LA, Lau H (2018) Microstructure and lifetime of Hf or Zr doped sputtered NiAlCr bond coat/7YSZ EB-PVD TBC systems. *Surf Coat Technol* 335:41–51
53. Lakiza SM, Tishchenko YaS, Redko VP, Lopato LM (2009) Al₂O₃-HfO₂-Y₂O₃ phase diagram, Isothermal sections at 1250 and 1650 °C. *Powder Metall Met Ceram* 48:225–233
54. Mercer C, Faulhaber S, Yao N, McIlwarth K, Fabrichnaya O (2006) Investigation of the chemical composition of the thermally grown oxide layer in thermal barrier systems with NiCoCrAlY bond coats. *Surf Coat Technol* 201:1495–1502
55. Spiridinov FM, Komissarova LN, Kocharov AG, Spitsyn VI (1969) The HfO₂-Y₂O₃ system. *Russ J Inorg Chem* 14:1332
56. Zhao C, Luo L, Xiao C, Zhao X, Wang X, Guo F, Xiao P (2018) The oxidation performance of plasma-sprayed NiAl bond coat: effect of Hf addition in bond coat and substrate. *Surf Coat Technol* 352:49–58
57. Barth TL, Marquis EA (2019) The effect of Ti on the early stages of oxidation of alumina-forming NiCrAl alloy. *Oxid Met* 92:13–26
58. Huang T, Naumenko D, Song P, Lu J, Quadackers WJ (2018) Effect of titanium addition on alumina growth mechanism on yttria-containing FeCrAl-base alloy. *Oxid Met* 90:671–690

Publisher's Note Springer Nature remains neutral with regard to jurisdictional claims in published maps and institutional affiliations.